Simulation

Simulations were created in various programs (mainly MATLAB and Java) to generate sample tomographic output graphics and compare the efficacy of prototype and scaled parabolic cavity model designs. Metrics such as temporal efficiency, cost efficiency, and maximum voxel resolution are taken into account.

$$\Delta p = \xi[ln(\frac{2mc^2\beta^2\gamma^2}{I}) + ln(\frac{\xi}{I}) + 0.2 - \beta^2 - \delta(\beta\gamma)]$$

$$\xi = (K/2)\langle Z/A\rangle(x/\beta^2)$$

Landau Vavilov Distribution

- Describes charged particle energy loss exhibited as those particles traverse mid to high thickness material cross sections
- Used to approximate energy losses exhibited by muons as they intersected the volumetric scintillator assembly

$$\frac{dI_\mu}{dE_\mu} \simeq 0.14(\frac{E_\mu}{GeV})^{-2.7}[\frac{1}{1+\frac{1.1E_\mu cos\theta}{115\ GeV}} + \frac{0.054}{1+\frac{1.1E_\mu cos\theta}{850\ GeV}}]$$

Gaisser's formula

- Empirical relation that expresses the rate of muonic flux variation with respect to the energy spectra and zenith angle
- Used to generate randomized muon events in conjunction with the proportion of the muon angular flux to the function $cos^2(\theta)$

$$dL = S \cdot \frac{dE}{1+k_B\frac{dE}{dx}}$$

Birks' law

- Describes the light emission as a function of energy deposition
- Used to approximate scintillation light yield

$$-\langle\frac{dE}{dx}\rangle = \frac{4\pi}{m_ec^2} \cdot \frac{nz^2}{\beta^2} \cdot (\frac{e^2}{4\pi\epsilon_0})^2 \cdot [ln(\frac{2m_ec^2\beta^2}{I\cdot(1-\beta^2)}) - \beta^2]$$

The Bethe-Bloch Equation

- Describes the energy lost per distance traveled by charged particles through a medium of atomic mass A, atomic number Z, and electron density n

Description of Methods

Six-stage stochastic model for generating muon scattering events

1. Muon trajectory generation
2. Muon propagation
3. Muon-scintillator interaction
4. Photon propagation and microcell interaction
5. Microcell behavior and preliminary signal generation
6. Trilateration algorithm and scan volume reconstruction

Relativistic physics

- Positional, velocity, and momentum-energy vector systems
- Lorentz transformation
- Time dilation for muon decay

SiPM attributes and behaviors

- Specifications of SiPM array from prototype
- Noise modelling with thermal, afterpulsing, and optical-crosstalk triggers
- Poisson distribution for thermal noise

Trilateration and tomographic imaging

- Map file constructed with localized material z-values
- Two-sample t-tests with variable significance thresholding
- 3D scan volume construction by accumulating confidence intervals for standard deviations of all muon scattering exhibited per voxel
- Power P of each muon scatter datapoint is scaled with muon momentum

Prototype and scaled-model comparison

- Differences in photon behavior interior to scintillator and dielectric medium boundary
- Algorithm to summate total photon retention

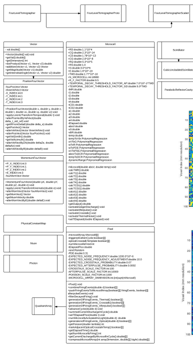

UML diagram of central classes in Monte Carlo simulation

$$N_{fired}(M,V,\lambda) = M\left(1-\exp\left(-\frac{PDE(V,\lambda)\cdot N_{ph}}{M}\right)\right)$$

Microcell Firing Rate

- SiPM behavior was modeled using an empirical formulation of photodiode output current as a function of time since an initial photoelectron induced avalanche

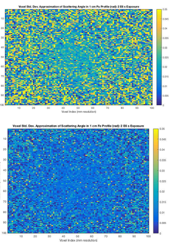

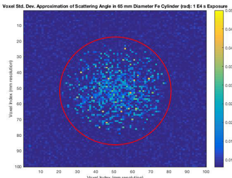

Simulation of 65mm diameter Fe disc situated on polystyrene base. The red annotation shows the outline of the disc as it appears in the scan field. Successful muon tracking is more frequent towards the center of the disc because the likelihood of the signal coincidence between all four sensor modules is maximized at that position due to net zenith and azimuth angle contributions from the empirical sea-level muon angular distribution. The simulated time exposure is 10,000 seconds, which coupled with the present voxel fill density demonstrates the low rate of data acquisition attributed to the scintillator spacing.

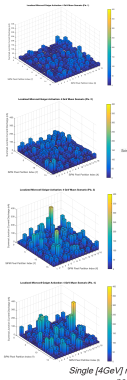

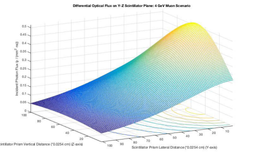

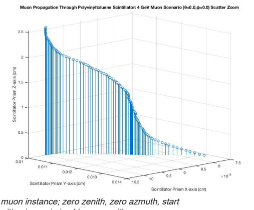

Single [4GeV] muon instance; zero zenith, zero azmuth, start position is maximized in x, y position

Thermal Noise and Scintillation Signal Comparison (without increased PDE)

2-Sample t-Test for 325MeV: 0.4140454519
2-Sample t-Test for 4GeV: 0.000089309481

- P-value of 0.414 is sufficiently high enough to fail to reject the assumption that the signal and noise current discharge distributions are equivalent at the minimally ionizing level. This merits the use of a peak-detection circuit instead of a raw ADC read-out setup.
- Low p-value of 0.0000893 displays evidence that we would be able to discern between thermal noise and the muon signal at the mean energy level.

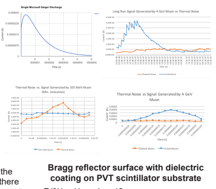

Weighing both cost and reflectiveness of the dielectric coating, it was determined that there would be four total layers of the dielectric coating. With four layers, 83.4% of the light given off from the scintillator would be received by the SiPM compared to <1% of the light which would have been received without incorporating a parabolic mirror. This mirror would reflect back 90.6% of the light given off from the scintillator; there would be a slight loss in light due to its attenuation through the scintillator.

Bragg reflector surface with dielectric coating on PVT scintillator substrate

- R(%) = (1-ne 1+ne)2
- ne = (nh)2p+2(nsnL)2p
- λedge = λ01
- (Delta) = 190arcsin(nh-nLnh+nL)
- TiO2: nh = 2.4
- MgF_2: nL = 1.19
- PVT: ns
- P = 4
- R(%) = 90.6%

Conclusion

We have sought to patent our novel approach to muon scattering tomography with the method of trilateration for locating incident muons. We are currently patent pending with a provisional patent, and we plan on taking further action in the near future to secure a full utility patent.

According to the Monte Carlo simulation described above which models the time efficiency of the prototype design, a cubic millimeter level of voxel resolution (which corresponds to 79,375 z data points) we can achieve at least 95% certainty of the mean muon scattering angle and 95% of the scan volume in 41 hours 43 minutes and 31 seconds. This estimate takes into account that 6.23% of the available angular distribution of muons will intersect all 4 scintillators. For the parabolic optical cavity design addendum, it is estimated that the analogous time efficiency of an equivalent scan volume and voxel resolution would be 29 minutes and 21 seconds, due to the increase in photon retention as observed by the SiPM to 83.4% versus a mere 0.58% in the uncladded scintillator concept.

Compared to typical muon-scattering tomography devices that utilize drift chambers in a six-planar formation, our design only requires three scintillating prismatic planes to measure muon trajectory. In addition, the cost of three plastic scintillators is significantly less than the cost of drift tubes. For instance, the cost of our novel design (uncladded) would be approximately 96.2% less expensive than the recent drift tube implementation outlined in Tomographic Imaging with Cosmic Ray Muons (Morris, 2008). Specifically, for an automobile counting station sized 4m x 4m x 5m (also described in Morris, 2008), the traditional cost of 3 million dollars for the six drift tube planes would fall to an estimated $115,000 using solid state volumetric scintillators coupled with SiPM arrays (with uncladded scintillator design).

Parabolic optical cavity pricing estimate results: For the parabolic optical cavity scintillator cladded with a dielectric coating to increase overall PDE, the pricing estimate for the milling of the PVT is $345, and the anticipated pricing for the application of a MgF_2/TiO_2 dielectric coating is $1310 for the surface area of 28.18 cubic centimeters. The ratio of pricing between the parabolic optical cavity design and the uncladded cube design is 16.07, however the ratio of time efficiencies is 42.53. Therefore, the time efficiency to cost ratio of the design addendum is 2.65, meaning that in any application, 2.65 times as many scan volumes may be processed at an equivalent pricing base.

Applications of Muon Tomography

- Nuclear waste monitoring
  - Dry cask storage
- Distinguishing radioactive materials from metals
  - Capable of detecting radioactive sources hidden under high density metals
- Carbon sequestration
  - Monitor rock density surrounding CO_2 injection sites
- Cargo inspection
  - Scan the inside of cargo to detect possible nuclear threats
- Geological surveying
- Structure stability monitoring
  - Welding inspection